doi: 10.56761/EFRE2022.S6-P-017001

Computer simulation of multi-gigawatt magnetic compression lines

V. Patrakov[1,2,*], *S. Rukin*[1]

[1]*Institute of Electrophysics UB RAS, Yekaterinburg, Russia*
[2]*Ural Federal University, Yekaterinburg, Russia*
[*]*vitpatrakov@gmail.com*

Abstract. Magnetic compression lines (MCL) are novel solid-state devices for multi-gigawatt sub-nanosecond and picosecond pulse amplification. Their operation is based on the interaction of magnetic field created by a powerful nanosecond or sub-nanosecond pulse with the magnetization vector in a ferrite medium. In this study a numerical model of an MCL was created, based on Maxwell's equations and Landau-Lifshitz-Gilbert equation for magnetization dynamics. The equation system is solved using COMSOL Multiphysics simulation software. The model shows good agreement with the experimental data. Using the created model, the process of power amplification in MCL was analyzed in terms of magnetic field and magnetization vectors. Based on this analysis, the mechanism of unipolar pulse amplification has been proposed.

Keywords: solid-state pulsed power, high-power picosecond generators, magnetic compression lines, numerical simulation.

1. Introduction

Non-linear transmission lines (NLTL) filled with saturated ferrite are promising solid-state sources of high-power microwave radiation. Such NLTLs are usually called gyromagnetic NLTLs (GNLTLs) because their operation principle is based on gyromagnetic precession of magnetization vector $\boldsymbol{M}$ in ferrite, which is magnetized into the state of deep magnetic saturation [1, 2]. A GNLTL typically consists of a coaxial transmission line, partially or fully filled with ferrite material, and an external magnetic bias circuit. The bias circuit creates axial saturating H-field, denoted as H_z. When a high voltage unipolar nanosecond pulse travels through such GNLTL, the azimuthal magnetic field H_θ, created by the current pulse, causes a gyromagnetic precession of the magnetization vector in the ferrite. This precession modulates the traveling wave with high-power oscillations of microwave frequency. At present, such GNLTLs can provide microwave generation at frequencies as low as 1 GHz and as high as 20 GHz [3], with typical pulsed RF power being in 10–100 MW range.

In recent years it has been observed that GNLTLs can also increase the peak power of unipolar pulses in the multi-gigawatt power range [4–6]. A GNLTL operating in this regime is called Magnetic Compression Line (MCL). In MCL, the incoming pulse is approximately equal in duration to a single period of the oscillations generated by the gyromagnetic precession. This condition allows the first half-cycle of the generated oscillations to effectively be used as a shorter, more powerful pulse. The theoretical estimate for a maximum coefficient of voltage amplification for MCL is $\sqrt{2}$. To date, the highest reported pulse power achieved using the MCL approach is 77 GW at 48-Ω load, with the pulse amplitude of 1.93 MV and pulse duration of 105 ps (FWHM) [6]. Contrary to typical spark-gap-based picosecond sharpeners, MCL operates without any switching elements, amplifying the pulse during its propagation through the line. This eliminates usual time limitations associated with spark gap switching time and allows to smoothly transition to picosecond megavolt pulse domain.

The development of MCL approach creates the need to accurately predict the operation of designed MCL stages and to study the underlying physical processes; hence, a numerical model of MCL device is needed. In literature there are reports on numerical models of GNLTLs, which are usually based on one of the two approaches. Several models [7, 8] consider the GNLTL as a transmission line, which can be described by the telegraph equations. The magnetization dynamics is solved using the Landau-Lifshitz-Gilbert equation (LLG) for a magnetized medium. Other models implement a more generalized approach [9–11], in which the line is solved as an electrodynamic structure using a full set of Maxwell's equations, while the magnetization dynamics is solved using

LLG equation. In present study it was decided to create a numerical model for the MCL using Maxwell's equations to solve the electrodynamic part of the model, and LLG equation to solve the precession of magnetization vector $\boldsymbol{M}$ in ferrite. The resulting coupled system is solved using COMSOL Multiphysics numerical simulation software [12].

2. Numerical model

To solve the propagation of an electromagnetic wave inside the coaxial line, Maxwell's equations were used. Using magnetic vector potential $\boldsymbol{A}$, defined as (curl $\boldsymbol{A}$) = $\boldsymbol{B}$, and defining static electric potential to be $\varphi = 0$ (Weyl/Gibbs/temporal gauge), the Maxwell's system can be rewritten as one $\boldsymbol{A}$-dependent equation (1):

$$\frac{1}{\mu_0}\nabla\times\left(\nabla\times\boldsymbol{A}-\mu_0\boldsymbol{M}\right)+\sigma\frac{\partial\boldsymbol{A}}{\partial t}+\varepsilon_0\varepsilon\frac{\partial^2\boldsymbol{A}}{\partial^2 t}=0\,. \tag{1}$$

Here $\mu_0 = 4\pi\cdot 10^{-7}$ H/m is permeability of free space, $\boldsymbol{M}$ is the magnetization of the medium, σ is electrical conductivity of the medium, $\varepsilon_0 = 8.854\cdot 10^{-12}$ F/m is permittivity of free space, ε is relative permittivity of the medium. As can be seen, such formulation assumes time-independent permittivity, i.e. no dielectric dispersion in dielectric medium. On the other hand, the magnetization term $\boldsymbol{M}$ is fully adjustable and can be set to account for any needed magnetization dynamics.

The magnetization dynamics for ferrite in a saturated state can be described using the Landau-Lifschitz-Gilbert equation (2):

$$\frac{d\boldsymbol{M}}{dt}=-\gamma\mu_0\left[\boldsymbol{M}\times\boldsymbol{H}_{eff}\right]+\frac{\alpha}{M_S}\left[\boldsymbol{M}\times\frac{d\boldsymbol{M}}{dt}\right]. \tag{2}$$

Here γ is electron gyromagnetic ratio, taken as $1.76\cdot 10^{11}$ rad/(s·T), $\boldsymbol{H}_{eff}$ is effective magnetic field experienced by the magnetic medium, M_s is the magnitude of saturation magnetization of the medium, and α is Gilbert's dimensionless damping coefficient, which usually is on the order of 0.01–0.1. The first term on the right-hand side of this equation has the physical meaning of a torque experienced by the magnetization in external magnetic field. This torque in a lossless case would cause the magnetization $\boldsymbol{M}$ to continuously precess around the vector $\boldsymbol{H}_{eff}$. The second term is damping term, which rotates the torque to some degree in the direction of $\boldsymbol{H}_{eff}$, which causes the precession to fade over time, eventually leading to the magnetostatic case, where $\boldsymbol{M}$ is aligned with $\boldsymbol{H}_{eff}$. Overall, the result of this process is that when the magnetic field is rapidly changed to a new direction, the $\boldsymbol{M}$ vector follows it, precessing around the new equilibrium state, until it fully aligns to the new position of $\boldsymbol{H}_{eff}$.

Equations (1) and (2) describe the dynamical part of the system. To find the initial distribution of bias H-field, a preliminary calculation is performed, which solves the magnetostatic equation to find the distribution of $\boldsymbol{H}_{bias}$ in the ferrite, created by a solenoid of a known geometry.

The described system of equations is solved using COMSOL Multiphysics numerical simulation software. To couple the system, $\boldsymbol{M}$ from the equation (2) is substituted into equation (1) as $\boldsymbol{M}$ in the curl term. $\boldsymbol{H}_{eff}$ in equation (2) includes $\boldsymbol{H}$ found from equation (1), as well as $\boldsymbol{H}_{bias}$ found at the preliminary step. In the general case, $\boldsymbol{H}_{eff}$ must also include the demagnetizing field $\boldsymbol{H}_d$, which arises due to boundary conditions whenever a magnetized sample is put into an external magnetic field. This field reduces the actual H-field in the sample. The demagnetizing fields can also be induced as a result of the change in magnetic flux inside the line, such as when $\boldsymbol{M}$ changes its direction. Because both $\boldsymbol{H}$ and $\boldsymbol{H}_{bias}$ are found as a direct result of solving Maxwell's equations with appropriate boundary conditions, the demagnetizing fields are automatically taken into account and no additional terms is needed.

Using this equation system, the model was created in two geometrical versions: 2D-axisymmetric (with the assumption of $\partial/\partial\varphi = 0$ for all variables, φ being the azimuthal angle), and full 3D. The advantage of the 2D model is a much lower computation time, while its obvious disadvantage is the inclusion of axisymmetric effects only. The outer and inner conductors of the coaxial line were modeled as a perfect electric conductor (PEC). At the boundary of the ferrite domain, the Brown boundary condition should be enforced, which is $\partial \boldsymbol{M}/\partial \boldsymbol{n} = 0$, $\boldsymbol{n}$ being a unit vector normal to the boundary. However, the default "zero flux" boundary condition provided by COMSOL at the boundaries of partial-differential-equation domains has the exact same physical meaning of a boundary which is impenetrable to the variable, in this case $\boldsymbol{M}$, so no additional conditions need to be applied.

3. Comparison with experimental data

The created model was verified against the experimental data for MCL3 [5] and MCL4 [6] lines. To get a better qualitative and quantitative match, some of ferrite parameters in the model were optimized, given the natural spread in their values and the absence of specification of these parameters by the manufacturer. Namely, these parameters were: saturation magnetization M_s, Gilbert's damping coefficient α, ferrite permittivity ε_f, and a total loss coefficient k_{loss}, which was added as a scaling factor to the output pulse, to describe the attenuation of the pulse caused by the line losses ($k_{loss} = 0$ – no losses, $k_{loss} = 1$ – complete attenuation). For both lines optimal parameters were found to be: $M_s = 310$ kA/m, $\alpha = 0.20$, $\varepsilon_f = 14.5$, $k_{loss} = 0.050$. The comparison of the experimental waveform of the output pulse and a calculated one is shown in Fig.1a for MCL3 and in Fig.1b for MCL4. As can be seen, for MCL3 the model provides a good agreement with experimental data in shape, amplitude, and relative delay of main and secondary peaks of the output pulse. For MCL4 qualitative agreement of the total pulse shape can be seen, with good quantitative agreement in the region of the main peak.

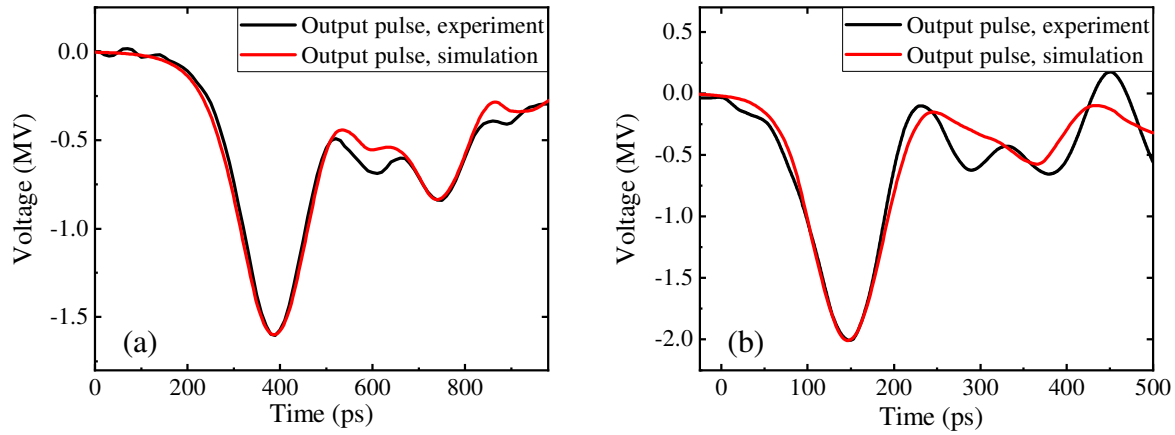

Fig.1. Comparison of experimental data and simulated waveform: (a) for MCL3, (b) for MCL4.

In the process of optimization, some dependencies of pulse parameters on material parameters were observed. A very weak dependence on α was noted in the range of 0.001–0.2. Increasing α in the 0.2–0.8 range leads to a noticeable decrease in pulse amplitude. The values of M_s and ε_f are in good agreement with the ones usually given in NLTL papers, such as [3, 9, 10]. The value of ε_f has a direct influence on a relative delay between the two peaks of the output pulse, with higher values leading to higher delay. Higher values of ε_f also correspond to larger FWHM durations of the main peak. Increase in M_s leads to somewhat shorter main peak of the output pulse, increase in its amplitude, and a drop in the voltage level of the quasi-plateau between the peaks. Another factor that

affects the details of pulse shape was found to be the geometry of the external magnetizing solenoid, or, in other words, the spatial distribution of the bias field vector $\boldsymbol{H}_{bias}$. The value of k_{loss} is also realistic and agrees with known attenuation coefficients for picosecond pulses in coaxial lines.

To compare the pulse evolution over the length of the MCL with the experimental data, a set of waveforms was experimentally obtained from MCL4, changing the number of ferrite rings in the MCL, i.e. changing the length of the amplifying section. The highest number of rings N = 88 corresponds to the ferrite section length of 352 mm. The same experiment was simulated in the created model. The results of theoretical calculation and experimental data are shown in Fig.2 as power waveforms. For each number of rings an experimental waveform is shown as a solid line, and a simulated one as a dashed line. As can be seen, the simulated and experimental dynamics of pulse amplification are in good agreement with each other.

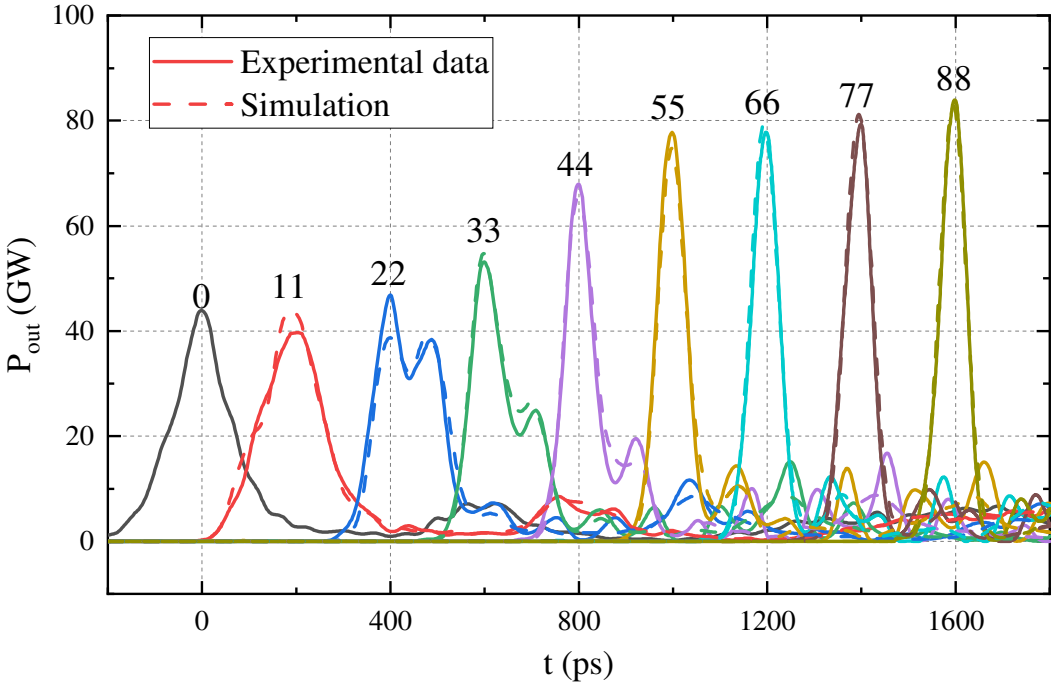

Fig.2. The process of pulse transformation along the MCL4: comparison of experimental data and simulation. The number above each waveform denotes the number of ferrite rings used.

4. Dynamics of power amplification process

The created model allows studying the dynamics of all the vector quantities in the MCL, which gives us the insight into the process of power amplification. For example, we will consider the process of power amplification in the MCL4 line. The quantities of interest are longitudinal magnetic field component H_z, azimuthal magnetic field component H_θ, magnetization $\boldsymbol{M}$, and a total H-field vector $\boldsymbol{H}_{eff}$. Fig.3a shows the simulated waveform of the pulse as it passes the cross-section of the MCL with the longitudinal coordinate z = 200 mm from the beginning of the ferrite. Fig.3b shows the directions of mentioned vectors at the time points A–D, as marked on the waveform.

The basic principle of power amplification in MCL is the induction of additional voltage across the line conductors by the change in magnetic flux produced by $\boldsymbol{M}$ vector. The reason for the appearance of the voltage in addition to the counter-EMF, which is always induced by the main pulse current, is the lag between the movement of $\boldsymbol{M}$ and $\boldsymbol{H}_{eff}$, which can be described by a divergence angle between these vectors α_{MH}. Modifying the analysis performed in [8] for arbitrary α_{MH} values, and assuming a steady precession of $\boldsymbol{M}$ around $\boldsymbol{H}_{eff}$ with an angular frequency ω, the additional instantaneous induced voltage V_i can be written as (3):

$$V_i = \mu_0 \cdot (R_f - r_f) \cdot \Delta z \cdot \omega \cdot M_S \cdot \sin \alpha_{MH} \cdot \frac{H_Z}{\sqrt{H_\theta{}^2 + H_Z{}^2}} \cdot \sin(\omega t) \tag{3}$$

where R_f and r_f are the outer and inner radii of ferrite filling respectively and Δz is a small arbitrary sampling step along MCL length, coming from the fact that equation (3) is derived using transmission line theory. As can be seen, the induced voltage is proportional to the ferrite filling factor of the line, the frequency of precession, saturation magnetization M_s, sine of α_{MH} angle, and the relation between bias H-field and pulse H-field in a form of field factor $H_z/(H_\theta{}^2+H_z{}^2)^{0.5}$.

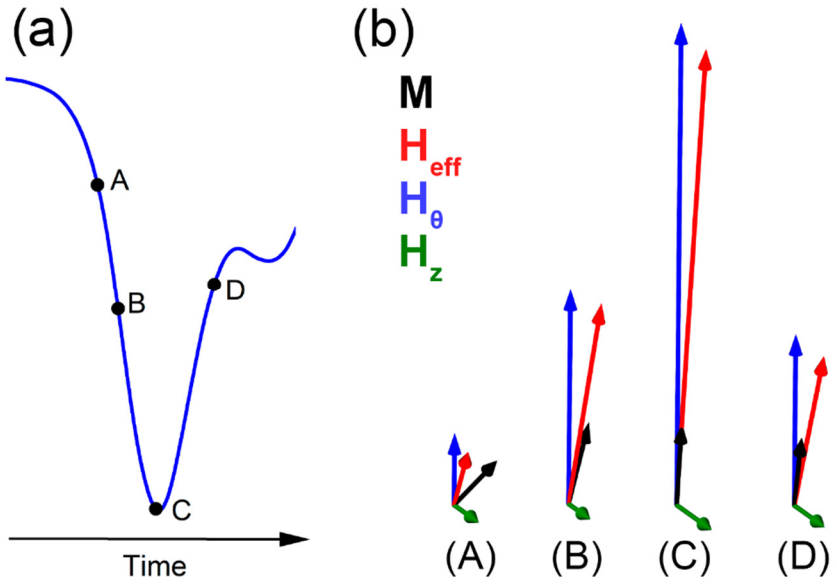

Fig.3. (a) waveform of the voltage pulse at coordinate z = 200 mm; (b) corresponding positions of vectors of interest at time points A, B, C, D.

From the formula (3) and Fig.3 the dynamics of the pulse amplification appears as follows. When the wave front of the pulse arrives at the cross-section of interest, the effective field $\boldsymbol{H}_{eff}$ starts changing in both magnitude and direction. The magnetization $\boldsymbol{M}$ follows $\boldsymbol{H}_{eff}$, but with some delay, which at first creates an angle α_{MH} of about 20 degrees between $\boldsymbol{M}$ and $\boldsymbol{H}_{eff}$ (point A). This causes the voltage V_i to be induced, which increases the amplitude of the front of the traveling pulse. When the main body of the pulse arrives, the field factor becomes much smaller, because H_θ corresponding to the peak of the pulse is about 10 times bigger than H_z. Simultaneously, such an increase in $\boldsymbol{H}_{eff}$ causes the M to follow it much more quickly, and the α_{MH} angle reduces to 1–5 degrees (points B, C, D). These two factors, in accordance with formula (3), hinder further voltage induction, effectively ending the process of power amplification.

The main difference of the described mechanism from a classical GNLTL operation seems to be in the time dependence of the induced voltage, caused by the difference in the relation of bias field and pulse field. In GNLTL the pulse field and bias field amplitudes are similar, with field factor $H_z/(H_\theta{}^2+H_z{}^2)^{0.5}$ being close to 0.5–0.7, and so the induced voltage takes a form of a decaying sine wave, leading to the induction of microwave oscillations. On the other hand, in MCL the amplitude of the driver pulse is much larger than in GNLTLs, which provides the field factors of 0.1 and lower, which effectively stops the induction process at times following the pulse front. This leads to a unipolar induced voltage wave traveling alongside the main pulse, which allows effective amplification of the main peak of the pulse. Thus, the dynamics of pulse formation in GNLTLs occurs

over the duration of several precession periods, while the dynamics of pulse formation in MCLs happens during a single precession turn.

5. Conclusion

In this study, a numerical model of a multi-gigawatt magnetic compression line was created using COMSOL Multiphysics simulation software. The created model shows a good agreement with experimental data, accurately predicting the overall shape of the output pulse and relative positions of main and secondary peaks, as well as the dynamics of the pulse amplification along the line. The model has allowed to study in detail the dynamics of magnetic field vector $\boldsymbol{H}_{eff}$ and magnetization vector $\boldsymbol{M}$ during the process of power amplification in the MCL. The observed behavior of the vectors shows that the increase in peak power of the pulse can be associated with the induction of additional voltage across the line conductors at the beginning of the first turn of the gyromagnetic precession. Further induction is then minimized by high amplitude of the *H*-field in the main body of the pulse, which leads to an effective unipolar power amplification of the driver pulse.

6. References

[1] Romanchenko I.V., Ulmaskulov M.R., Sharypov K.A., Shunailov S.A., Shpak V.G., Yalandin M.I., Pedos M.S., Rukin S.N., Konev V.Y., Rostov V.V., *Rev. Sci. Instrum.*, **88**, 054703, 2017; doi: 10.1063/1.4983803

[2] Bragg J.W.B., Dickens J.C., Neuber A.A., *IEEE Trans Plasma Sci*, **41**(1), 232, 2013; doi: 10.1109/TPS.2012.2226169

[3] Ulmaskulov M.R., Shunailov S.A., *J. Appl. Phys*, **130**(23), 234905, 2021; doi: 10.1063/5.0072352

[4] Gusev A.I., Pedos M.S., Ponomarev A.V., Rukin S.N., Timoshenkov S.P., Tsyranov S.N, *Rev. Sci. Instrum.*, **89**, 094703, 2018; doi: 10.1063/1.5048111

[5] Alichkin E.A., Pedos M.S., Ponomarev A.V., Rukin S.N., Timoshenkov S.P., Karelin S.Y., *Rev. Sci. Instrum.*, **91**, 104705, 2020; doi: 10.1063/5.0017980

[6] Rukin S.N., Ponomarev A.V, Alichkin E.A., Timoshenkov S.P., Pedos M.S., Sharypov K.A., *Proc. 7th Int. Congr. on Energy Fluxes and Radiation Effects (EFRE)*, Tomsk, Russia, 92, 2020; doi: 10.1109/EFRE47760.2020.9241919

[7] Dolan J.E., *J. Phys. D*, **32**(15), 1826, 1999; doi: 10.1088/0022-3727/32/15/310

[8] Cui Y., Meng J., Huang L., Yuan Y., Wang H., Zhu D., *Rev. Sci. Instrum.*, **92**, 034702, 2021; doi: 10.1063/5.0040323

[9] Karelin S.Y., Krasovitsky V.B., Magda I.I., Mukhin V.S., Sinitsin V.G., *Plasma*, **2**(2), 258, 2019; doi: 10.3390/plasma2020018

[10] Huang L., Meng J., Zhu D., Yuan Y., *IEEE Trans Plasma Sci*, **48**(11), 3847, 2020; doi: 10.1109/TPS.2020.3029524

[11] Priputnev P., Romanchenko I., Tarakanov V., Pegel I., *Proc. 7th Int. Congr. on Energy Fluxes and Radiation Effects (EFRE)*, Tomsk, Russia, 434, 2020; doi: 10.1109/EFRE47760.2020.9241904

[12] COMSOL Multiphysics General-Purpose Simulation Software [online]; https://www.comsol.com/comsol-multiphysics